

Article

# Zirconium-Aluminum-Oxide Dielectric Layer with High Dielectric and Relatively Low Leakage Prepared by Spin-Coating and the Application in Thin-Film Transistor

Zhihao Liang<sup>1</sup>, Shangxiong Zhou<sup>2</sup>, Wei Cai<sup>1</sup>, Xiao Fu<sup>1</sup>, Honglong Ning<sup>1,\*</sup>, Junlong Chen<sup>1</sup>, Weijian Yuan<sup>1</sup>, Zhennan Zhu<sup>1</sup>, Rihui Yao<sup>1,2,\*</sup> and Junbiao Peng<sup>1</sup>

<sup>1</sup> State Key Laboratory of Luminescent Materials and Devices, South China University of Technology, Institute of Polymer Optoelectronic Materials and Devices, Guangzhou 510640, China; 201530291443@mail.scut.edu.cn (Z.L.); c.w01@mail.scut.edu.cn (W.C.); 201630343721@mail.scut.edu.cn (X.F.); 201664343704@mail.scut.edu.cn (J.C.); 201430320366@mail.scut.edu.cn (W.Y.); mszhuzn@mail.scut.edu.cn (Z.Z.); psjbpeng@scut.edu.cn (J.P.)

<sup>2</sup> Guangdong Province Key Lab of Display Material and Technology, Sun Yat-sen University, Guangzhou 510275, China; 201820117973@mail.scut.edu.cn

\* Correspondence: ninghl@scut.edu.cn (H.N.); yaorihui@scut.edu.cn (R.Y.)

Received: 8 February 2020; Accepted: 17 March 2020; Published: 18 March 2020



**Abstract:** In this paper, zirconium–aluminum–oxide (ZAO) dielectric layers were prepared by a solution method with intent to combine the high dielectric constant with a low leakage current density. As a result, dielectric layers with improved electrical properties as expected can be obtained by spin-coating the mixed precursor. The chemical and physical properties of the films were measured by thermogravimetric differential scanning calorimetry (TG-DSC), X-ray diffraction (XRD), X-ray photoelectron spectroscopy (XPS) and a UV spectrometer. It is observed that the oxygen defects and the hydroxide in the films are reduced with the addition of high-bond-energy zirconia, while the films can remain large optical band gaps thanks to the presence of alumina. The metal-insulator-metal (MIM) devices were fabricated, and it was seen that with a molar ratio of Zr:Al = 3:1 and an annealing temperature of 500 °C, the dielectric layer afforded the highest dielectric constant of 21.1, as well as a relatively low leakage current of  $2.5 \times 10^{-6}$  A/cm<sup>2</sup> @ 1 MV/cm. Furthermore, the indium–gallium–zinc oxide thin-film transistors (IGZO-TFTs) with an optimal ZAO dielectric layer were prepared by the solution method and a mobility of 14.89 cm<sup>2</sup>/Vs, and a threshold voltage swing of 0.11 V/dec and a  $6.1 \times 10^6$  on/off ratio were achieved at an annealing temperature of 500 °C.

**Keywords:** solution method; zirconium–aluminum–oxide; mixed precursor; high dielectric constant; metal oxide thin-film transistor

## 1. Introduction

As a basic unit, thin-film transistors (TFT) play an important role in displays [1–5], and the dielectric layer is the key for the TFT's electrical stability [6–9]. Due to their good transmittance, high dielectric constant and low temperature preparation, amorphous metal oxide dielectric layers have attracted widespread attention [10–13].

Vacuum methods such as magnetron sputtering—the usual process to prepare metal oxide thin-film transistors (MOTFT)—have been facing difficulties in lowering the high equipment costs and simplifying the complex production processes [14–17]. Therefore, the solution methods are widely focused on by scholars due to their simpler processing and lower expense. However, solution-processed dielectric layers have problems with unstable properties, owing to the large number of organic

residues [18–21]. Thus, with the ambition to improve the properties of the dielectric layers fabricated by spin-coating, a method of mixing has been employed as the mixed dielectric layer that, combined with the advantages of the mixed material, can obtain better electrical properties. What's more, the mixed component can solve the problem with a polycrystalline structure and a rough surface [22–24].

Shu Jiang [25] et al. adopted a solution-processed five-layer-stacked structure,  $\text{TiO}_2/\text{Al}_2\text{O}_3/\text{TiO}_2/\text{Al}_2\text{O}_3/\text{TiO}_2$  (denoted as TATAT), as the gate dielectric layer of the TFT, which greatly improved its mobility, owing to the smoother surface of the dielectric-channel interface and  $\text{TiO}_2$  surface. In their research, thinner layers of  $\text{TiO}_2$  were prepared to weaken the crystallization and deteriorate the surface morphology, with the thicker  $\text{Al}_2\text{O}_3$  interface layers introduced to the good electrical performance. Weihua Wu [26] dissolved  $\text{AlO}_x$  and  $\text{YO}_x$  precursors to produce an  $\text{AlO}_x:\text{Y}$  gate dielectric layer by spin-coating to reduce the thickness decrease brought from multi-cycle spin-coating routes. Equipped with a better surface flatness, the  $\text{AlO}_x:\text{Y}$  films demonstrate competitive insulating performance. As a result, the IGZO-TFT made of  $\text{AlO}_x:\text{Y}$  has good electrical properties (leakage current of  $8.2 \times 10^{-8} \text{ A/cm}^2$  @ 2 MV/cm and a dielectric constant of 7.4).

As with the examples mentioned above, aluminum oxide is the main component of the hybrid dielectric layers, as alumina has advantages of a high breakdown voltage and a low leakage current density, but the low dielectric constant limits its application in TFTs [27,28]. Though the mixed dielectric layers above have better electric properties, they still have problems with a large quantity of defects and low dielectric constants. Among various high-k dielectric materials, zirconia is well-known for its high bond energy, which is enable to reduce the oxygen defects in films [29,30]. Therefore, we intended to mix alumina with zirconia to reduce the defects in the films and improve the dielectric constant, and moreover, to realize the optimal performance of the dielectric layer.

Hence, the zirconium–aluminum–oxide (ZAO) film was prepared by mixing alumina with zirconia to obtain an insulating layer with a high performance. In this study, the precursors were prepared by dissolving zirconium nitrate pentahydrate and aluminum nitrate nonahydrate. The ZAO films were fabricated on substrates using the mixed precursors by spin-coating. The dielectric films were analyzed by X-ray diffraction (XRD), X-ray reflectivity (XRR) and a UV spectrometer. Based on these results, metal-insulator-metal (MIM) devices were fabricated to measure the dielectric constant and leakage current density. Then, the chemical compositions of the ZAO films were investigated by X-ray photoelectron spectroscopy (XPS) and the optimized parameters of the films were revealed. Finally, we prepared the IGZO-TFT devices with optimal ZAO dielectric layers.

## 2. Experimental Detail

### 2.1. Precursor Solution Synthesis

A 0.4 M zirconium–aluminum–oxide (ZAO) precursor was prepared by dissolving zirconium nitrate pentahydrate ( $\text{Zr}(\text{NO}_3)_4 \cdot 5\text{H}_2\text{O}$ ) and aluminum nitrate nonahydrate ( $\text{Al}(\text{NO}_3)_3 \cdot 9\text{H}_2\text{O}$ ) in of 2-methoxyethanol(2-MOE). The molar ratios of the ZAO precursor solution were Zr:Al = 4:0, 3:1, 1:1, 1:3 and 0:4. These solutions were stirred vigorously for 24 h, and were then aged under ambient conditions for 24 h.

### 2.2. Film Fabrication and Characterization

The surface tension and viscosity were measured by an Attension Theta Lite (TL200, Biolin Scientific, Gothenburg, Sweden). Thermogravimetric differential scanning calorimetry (TG-DSC) was used to measure the thermal behaviors of the precursor solution at a heating rate of  $10 \text{ }^\circ\text{C}/\text{min}$  from room temperature to  $600 \text{ }^\circ\text{C}$ .

The substrates were processed by UV/ozone at  $25 \text{ }^\circ\text{C}$  for 10 min. The mixed precursor was respectively spin-coated on the glass substrate at 5000 r/min for 30 s, and pre-annealed at 300, 400 and  $500 \text{ }^\circ\text{C}$  for 10 min. The spin-coating process was repeated three times before annealing for 2 h at various temperatures (300, 400 and  $500 \text{ }^\circ\text{C}$ ) corresponding to the pre-annealing temperature. The

transmissivity of ZAO films was investigated with a UV-VIS spectrophotometer (UV-3600SHIMADZU, Kyoto, Japan). The thicknesses and densities were measured by X-ray reflectivity (XRR) (EMPYREAN, PANalytical, Almelo, the Netherlands), and the surface morphology of the ZAO film was investigated by atomic force microscopy (AFM) (BY3000, Being Nano-Instruments, Guangzhou, China). X-ray photoelectron spectroscopy (XPS) (Thermo Fisher Scientific, Waltham, MA, USA) analysis was carried out to investigate the chemical composition of the ZAO thin films, with the carbon 1s peak (284.8 eV) as a calibration reference.

### 2.3. Metal-Insulator-Metal Device Fabrication and Characterization

A 150 nm-thick indium tin oxide (ITO) deposited by direct current (DC) sputtering on glass substrates was used as a bottom electrode. To measure the electrical characteristics of the ZAO films, we fabricated an MIM device comprising Al electrode/ZAO films/ITO substrates. The ZAO films were spin-coated on the ITO substrates, and the 100 nm-thick circular aluminum electrode was deposited by RF sputtering through a shadow metal mask. The current–voltage (I–V) and capacitance–voltage (C–V) characteristics of the MIM capacitor were measured by the Keithley4200 (Tektronix, Beaverton, OR, USA) parameter analyzer under ambient conditions.

### 2.4. Thin-Film Transistor Applications and Characterization

After spin-coating the ZAO films on the ITO substrates, the IGZO with 10 nm thickness was deposited by DC pulse sputtering with a pressure of 1 mTorr (O:Ar = 5%) and patterned by a shadow mask. The IGZO target is composed of the atomic ratio of In:Ga:Zn:O = 1:1:1:4. Then, the IGZO film was annealed at 300 °C for 1 h. At the end, the Al source/drain electrodes were deposited on it. The W/L ratio of the TFTs was 1.38. A semiconductor parameter analyzer (Agilent4155C, Agilent, Santa Clara, CA, USA) was used under an ambient atmosphere to evaluate the electrical characteristics of TFTs.

## 3. Result and Discussion

The thermogravimetry-differential scanning calorimetry (TG-DSC) measurement was performed to measure the thermal behaviors of the precursor solution, and the curves are shown in Figure 1. The curves of the mixed precursor with different ratios are similar. An endothermic peak is observed at around 135 °C [31], which is related to the evaporation of the solution, corresponding to the weight loss from the TG curve. In Figure 1a, the exothermic peak located at about 150 °C can be explained by the bonding of metal and oxygen, where a grid metal-oxide-structure was formed. The exothermic peak located at 330–340 °C can be attributed to the crystallization of zirconia, but in Figure 1b there is no crystallization peak in the DSC curve, since the crystallization temperature of alumina is above 600 °C.

The surface tension and viscosity of the precursors were measured, and the results are shown in Figure 1c. It can be seen that as the aluminum content increases, the viscosity and surface tension grow more and more rapidly when the ratio is above 3:1. It is known that suitable surface tension and viscosity allow a more uniform spreading, resulting in a smoother surface and improved performances of the dielectric layers. However, the excessive surface energy of the solution would cause a poor film formation [32,33]. From Figure 1c, the surface tension and viscosity of the precursors are excessive when the ratio is above 3:1. Therefore, the substrates were processed by UV to optimize the spin coating.

We set the annealing temperature to 300, 400 and 500 °C, in order to investigate not only the changes in the properties of the film before and after crystallization, but also the effect of temperature on the properties of the film. Moreover, to study the route the zirconia and alumina interact with each other as the mixing ratio changes, we spin-coated the films with different molar ratios of Zr:Al = 4:0, 3:1, 1:1, 1:3 and 0:4.

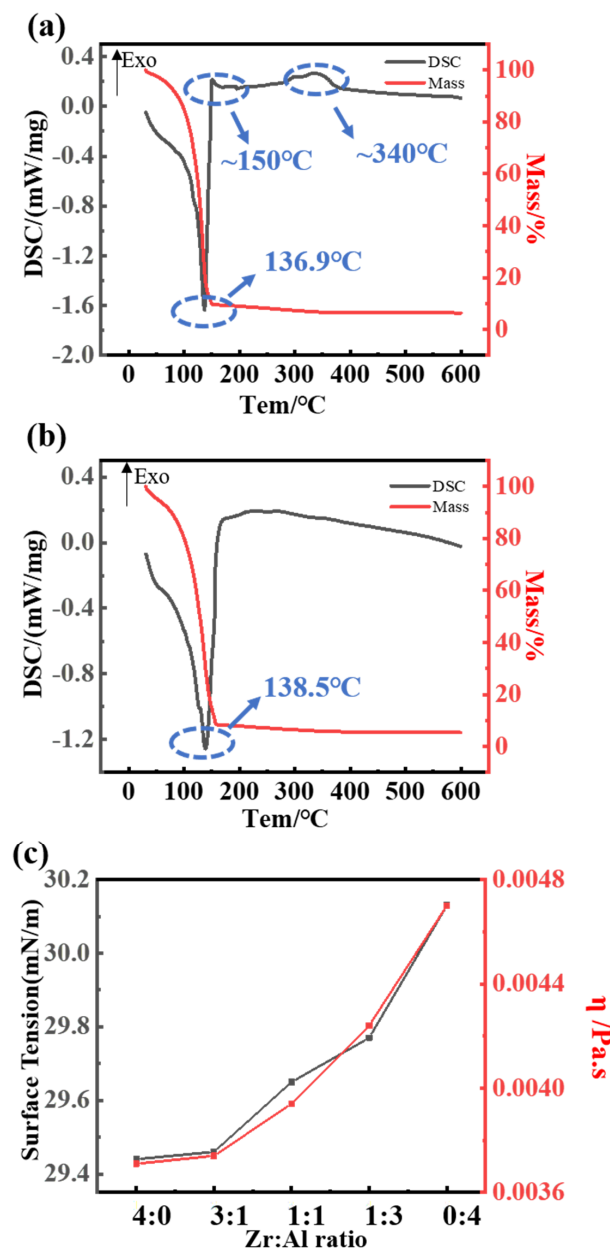


**Figure 1.** Thermal behavior of the ZAO precursor solution analyzed by thermogravimetry-differential scanning calorimetry (TG-DSC): (a) pure zirconia film; (b) pure alumina film; and (c) the surface tension and viscosity of the precursor with the various ratios.

X-ray reflectivity (XRR) measurements were carried out to measure the thicknesses and densities of the films with different ratios. From Figure 2, the thicknesses of the films with various ratios are similar at 300 °C. At 400 and 500 °C, the smaller thickness of the pure zirconium film may come down to the crystallization of zirconia [34]. Thicknesses then climb, due to the longer Al-O bond replacement Zr-O bond and the inhibition of dense crystalline structures. At the ratio of Zr:Al = 1:3 and 0:4, the thickness drops, possibly owing to the poorer film formation consistent with the growth of surface tension and viscosity. The result of density reveals that more organic residues, dangling bonds and hydroxyl were removed at higher annealing temperatures so the films were denser and thinner [35,36], which may come down to better electrical properties. Moreover, from the results above, we assumed that the addition of the alumina can break the dense crystal structure attributed to the inhibition effect on crystallization, which will be discussed as part of the X-ray diffraction (XRD) results.

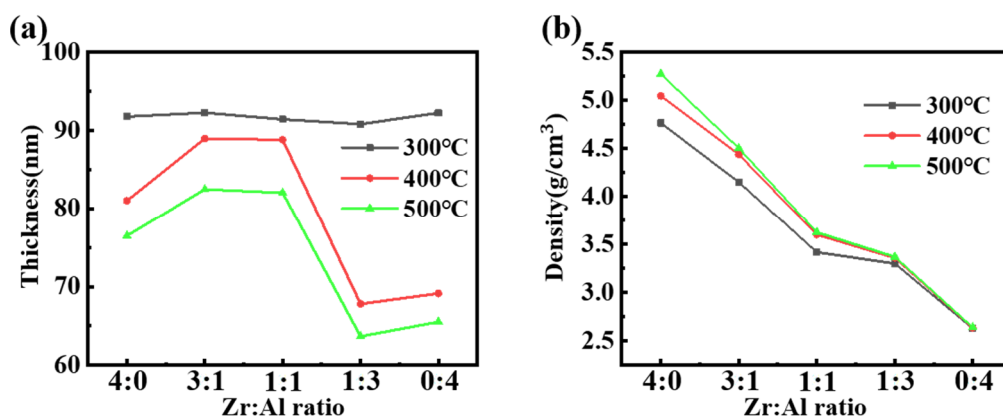


**Figure 2.** (a) The relationship among the thin film thickness, mixing ratio and annealing temperature and (b) the relationship among the thin film density, mixing ratio and annealing temperature.

In Figure 3b,c, films with a ratio of Zr:Al = 4:0 have obvious diffraction peaks located at 30.3°, which means zirconia crystal at 400 and 500 °C. Normally, an amorphous phase has advantages over a crystalline phase in obtaining a low leakage current, as the crystallization makes the conductive channel easier to form [37,38]. As the XRD patterns show, the ZAO films exhibit amorphous phases at 400 and 500 °C, which indicated that the addition of alumina can inhibit the crystallization of films above the crystallization temperature of zirconia, thereby reducing the films' leakage current density.

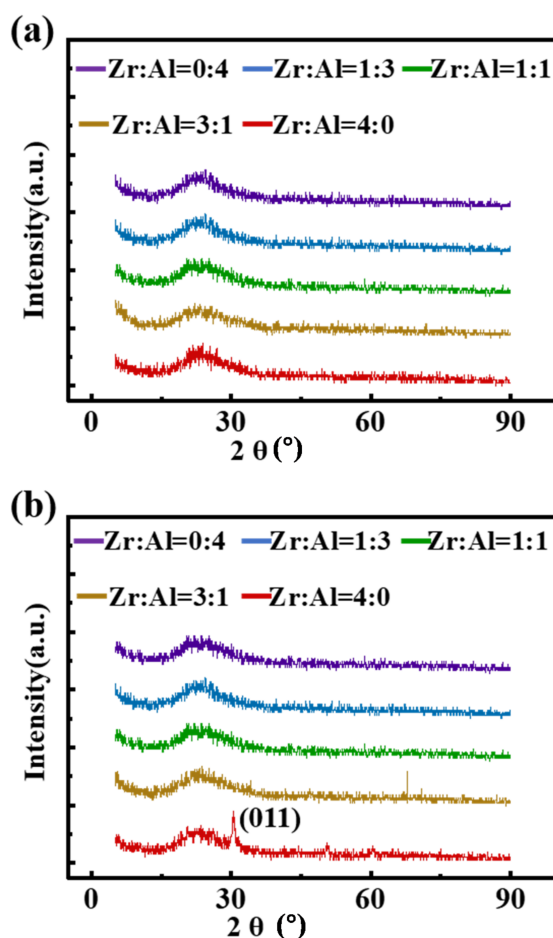
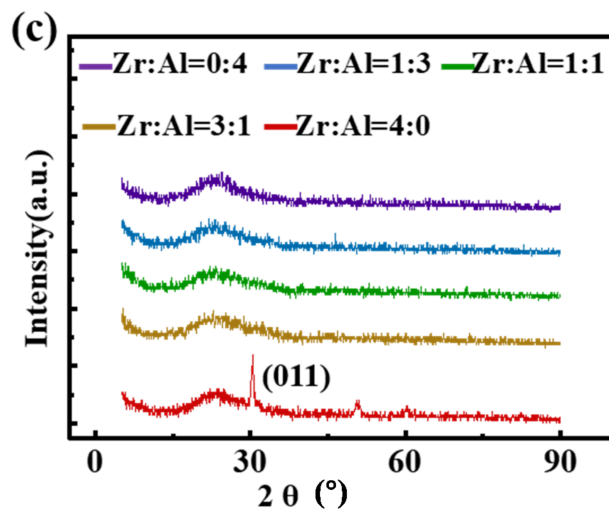
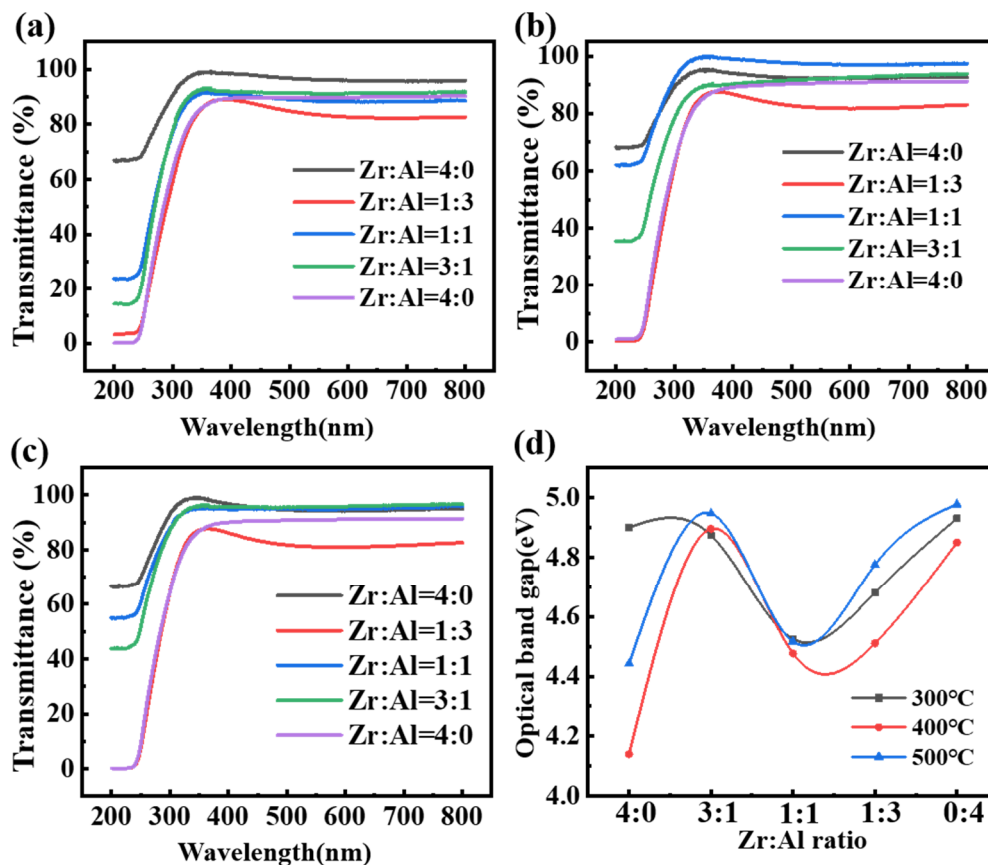


Figure 3. Cont.



**Figure 3.** XRD patterns of the ZAO films of different ratios annealed at: (a) 300 °C; (b) 400 °C; and (c) 500 °C, respectively.

Figure 4a–c reveals that all the films presented transmittance ratios of over 90% in the wavelength range of the visible light. Therefore, ZAO films are suitable for fabricating transparency devices.



**Figure 4.** Transmittance of the ZAO films of different ratios annealed at: (a) 300 °C; (b) 400 °C; and (c) 500 °C, respectively; and (d) optical bandgaps of the ZAO films changing with the mixing ratio of zirconia and alumina annealed at various temperatures.

The optical band gap of each film was calculated by the Tauc relationship [39] (1) on the base of the measurement of the transmittance. Take  $(\alpha h\nu)^2$  as the vertical axis and  $h\nu$  as the horizontal axis to make the curve, extend the linear part, and the intersection with the horizontal axis is  $E_g$

$$(\alpha h\nu)^2 = C(h\nu - E_g) \quad (1)$$

where  $C$  is constant for a direct transition,  $\alpha$  is the absorption coefficient and  $\nu$  is the frequency of the incident photon;

$$\alpha = -d^{-1}(\ln T) \quad (2)$$

$d$  is the film thickness and  $T$  is the transmittance;

$$h\nu = hc/\lambda \quad (3)$$

$\lambda$  is the wavelength for transmittance and  $h$  is Planck's constant ( $h = 4.13567 \times 10^{-15}$  eV·s,  $c = 3 \times 10^{17}$  nm/s).

The calculation results of the optical bandgap are exhibited in Figure 4d. The films with a ratio of Zr:Al = 3:1 achieved optical bandgaps (>4.8 eV) comparable to the pure alumina films, which is larger than the pure zirconia films (4.1 to 4.4). It can be confirmed that the alumina in the mixed film has the effect of improving the films' optical bandgap to obtain a lower leakage current density. This result is probably owing to the Burstein–Moss effect due to the mixing with Al. The Fermi level of zirconia will be inside the conduction band when it is mixed with Al. Therefore, the states in the conduction band are partly filled, and the absorption edge would shift to the higher energy [40,41].

X-ray photoelectron spectra (XPS) was used to clarify the chemical structures and compositions of the ZAO films with different mixing ratios at 400 °C. The peak at  $529.5 \pm 0.5$  eV is attributed to the bonded oxygen (M–O–M). The peak at ~532 eV is assigned to the bonded oxygen in the lattice defects and hydroxide(–OH) [42]. The contents of the various oxygen with different ratios are summarized in Table 1, while the tendency is concluded in Figure 5f. According to the spectral peak information shown in Figure 6, the mixing ratios of zirconium with aluminum in various samples were basically in line with expectations, and the results are shown in Table 2.

**Table 1.** The mixing ratios of Zr:Al according to the spectral peak information.

Designed Ratios of Zr:Al	3:1	1:1	1:3
The Ratios of Zr:Al From XPS	2.33:1	1:1.14	1:2.87

**Table 2.** The relative quantity of oxygen vacancies varied with the ratios.

Molar Ratio Zr:Al	Metal-Bonded Oxygen (~529.5 eV)	Oxygen Form the Lattice Defect (~532 eV)
4:0	88.37%	11.63%
3:1	76.11%	23.89%
1:1	69.00%	31.00%
1:3	67.16%	32.84%
0:4	71.93%	28.07%

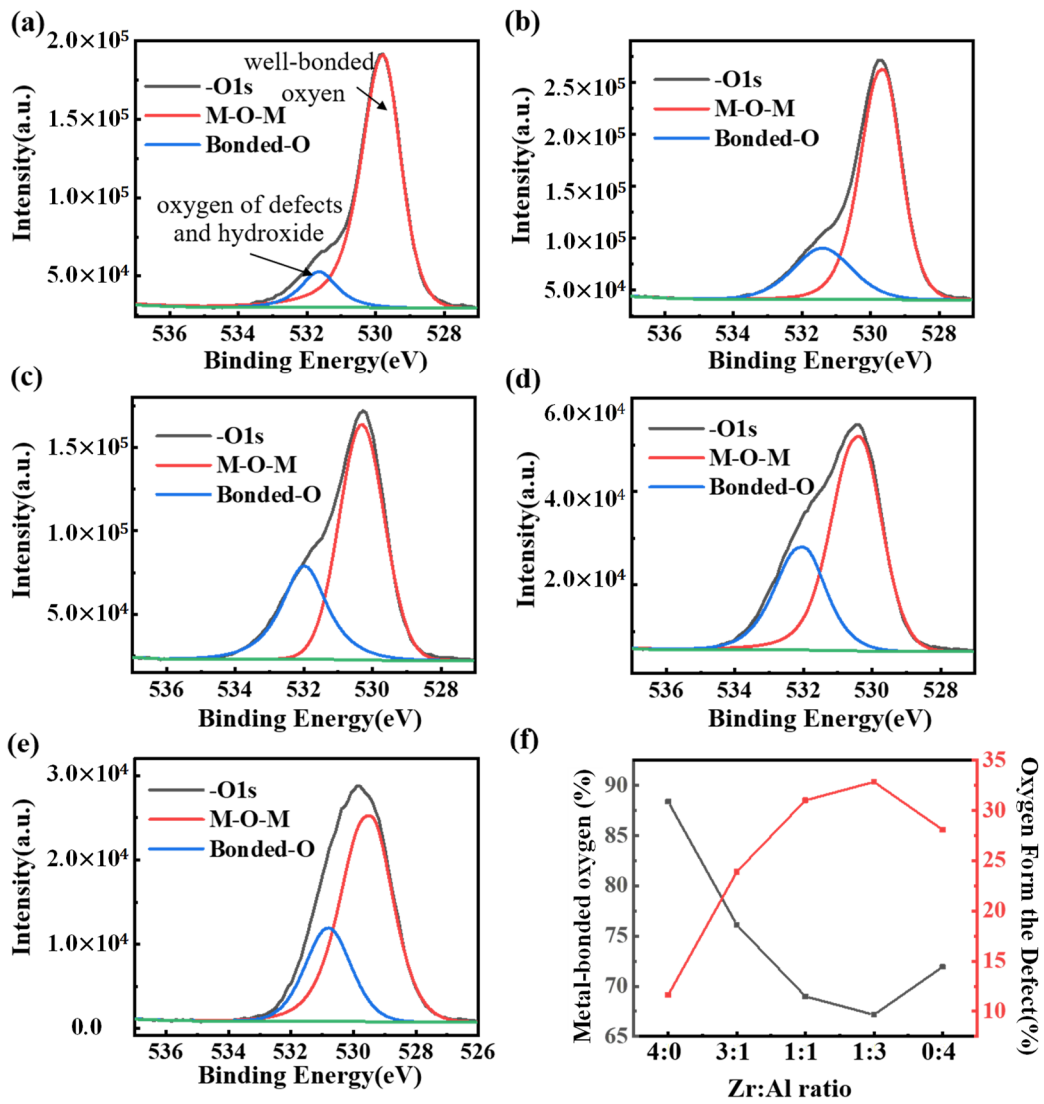


Figure 5. XPS spectra: (a–e) O 1s for different films (with molar ratios of Zr:Al = 4:0, 3:1, 1:1, 1:3 and 0:4) annealed at 400 °C; and (f) the tendency of oxygens as a function of the ratios.

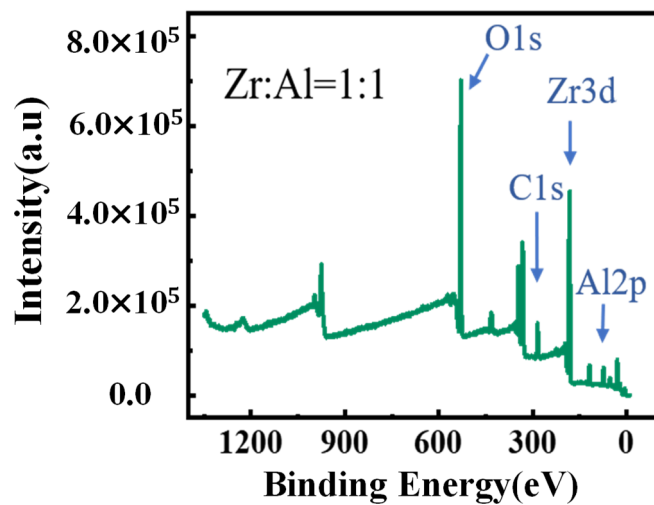


Figure 6. XPS spectra of overview scans for the ZAO (Zr:Al = 1:1) film.

Due to the stronger combination of zirconia, pure zirconia has fewer oxygen defects than pure alumina. As the weakly bonded oxygen with aluminum is replaced by the stably bonded oxygen with zirconium, hydroxide and oxygen defects are more difficult to form. For this reason, the metal-bonded oxygen contents of the ZAO films drops with the increase of zirconia. However, since zirconia would crystallize below 400 °C, the incorporation of zirconia promotes the formation of a low-temperature oxide lattice of alumina [43]. As a result, the addition of zirconia would give rise to a larger number of bonded oxygens in films with the ratios of Zr:Al = 1:1 and 1:3.

On this base, metal-insulator-metal (MIM) devices were fabricated, and we then characterized the electrical properties as a gate dielectric.

From Figure 7, the ZAO films show the higher leakage currents than the pure zirconia film at the 300 °C annealing temperature. This is the opposite at 400 °C and 500 °C, as the addition of alumina can reduce the leakage current density of the ZAO-mixed film, consistent with the inhibition of crystallization and the accretion of optical bandgaps. As the annealing temperature increases, the dielectric layers achieved lower leakage current densities—except pure zirconia films—because of the crystallization. Therefore, as for the ZAO films, a better performance can be attained by increasing the annealing temperature. The pure alumina films show the lowest leakage current, but with lower relative dielectric constants, which is discussed in the result of the relative dielectric constants. What's more, it has been found that at 400 °C and 500 °C, films with a molar ratio of Zr:Al = 3:1 have the lowest leakage current ( $1.35 \times 10^{-6}$  and  $2.5 \times 10^{-6}$  A/cm<sup>2</sup> @ 1 MV/cm at 400 and 500 °C) among the ZAO films, owing to their large thickness and optical bandgap.

The capacitance values are shown as a function of voltage in Figure 8a–c. The dielectric properties of ZAO films with a ratio of Zr:Al = 1:1 and 1:3 show instability versus voltage, which should be attributed to the high content of the bonded oxygen, as more water was absorbed [44]. The relative dielectric constants were calculated on the base of the C-V curves. According to the relative dielectric constants shown in Table 3, the dielectric layers with the ratios of Zr:Al = 1:1 and 1:3 achieve the maximum relative constants (41.1 to 292). The higher dielectric constants are mainly due to the presence of a large amount of defects (>30%), according to the XPS results, and the defects create more carriers, such as oxygen vacancies, in the microstructure of metal oxides, which accumulate more electric charges at two sides of boundary layers [45]. Nevertheless, as a consequence, a relatively high leakage current density (almost  $10^{-4}$  A/cm<sup>2</sup> @ 1 MV/cm) is obtained, as shown in Figure 7a–c, which make the films incompatible with high performance TFTs. Therefore, we only compared the dielectric constants of the pure metal oxide films with the ZAO films with a ratio of Zr:Al = 3:1. It is shown in Figure 8d that ZAO films have higher relative dielectric constants than pure alumina films. When the weak Al-O bond (511 J/mol) [22] is replaced by a strong Zr-O bond (776.1 J/mol), the oxygen defects have more difficulty in forming. The relatively higher dielectric constants are mainly due to the smaller quantity of oxygen defects. With a molar ratio of Zr:Al = 3:1, zirconia can reduce bonded oxygen in the film, leading to a higher dielectric constant than that of pure alumina films. What's more, an increasing temperature results in a higher dielectric constant as more defects are removed.

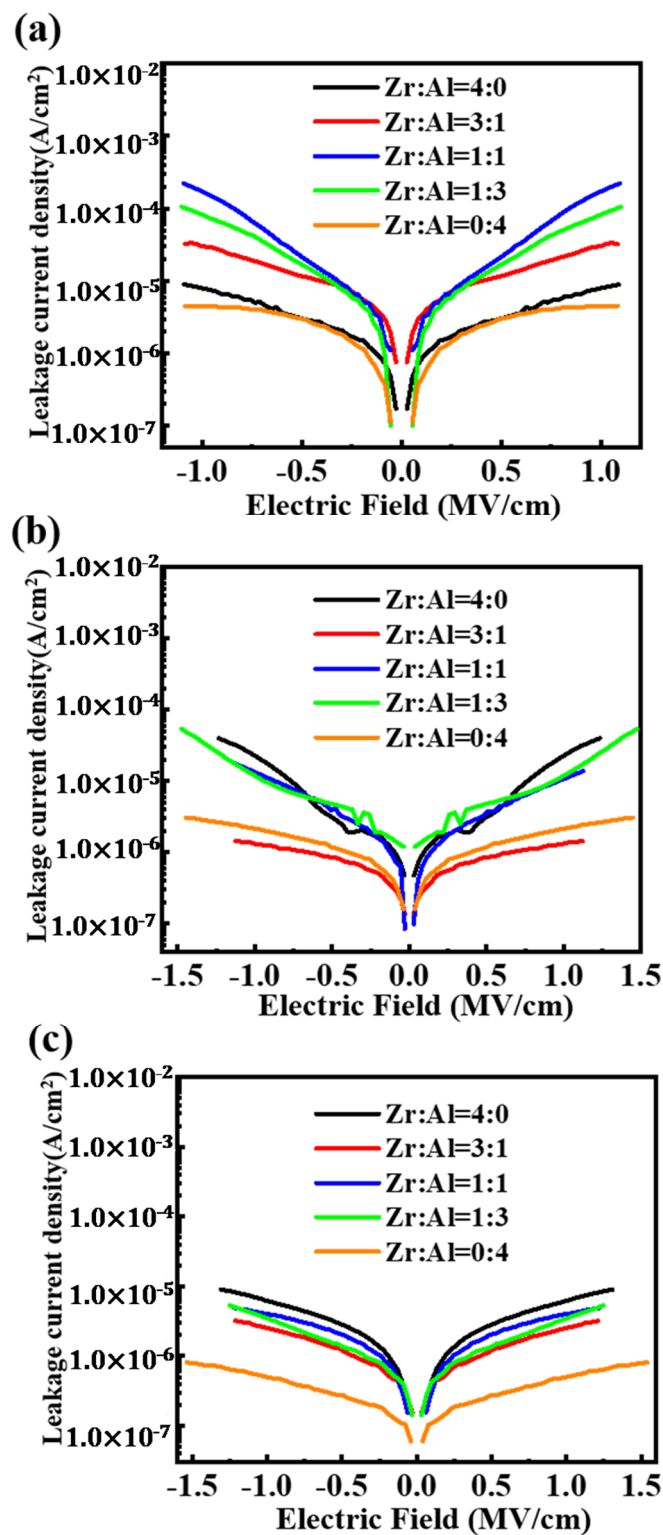


**Figure 7.** The leakage current densities of the ZAO films with altering ratios annealed at: (a) 300 °C; (b) 400 °C; and (c) 500 °C.

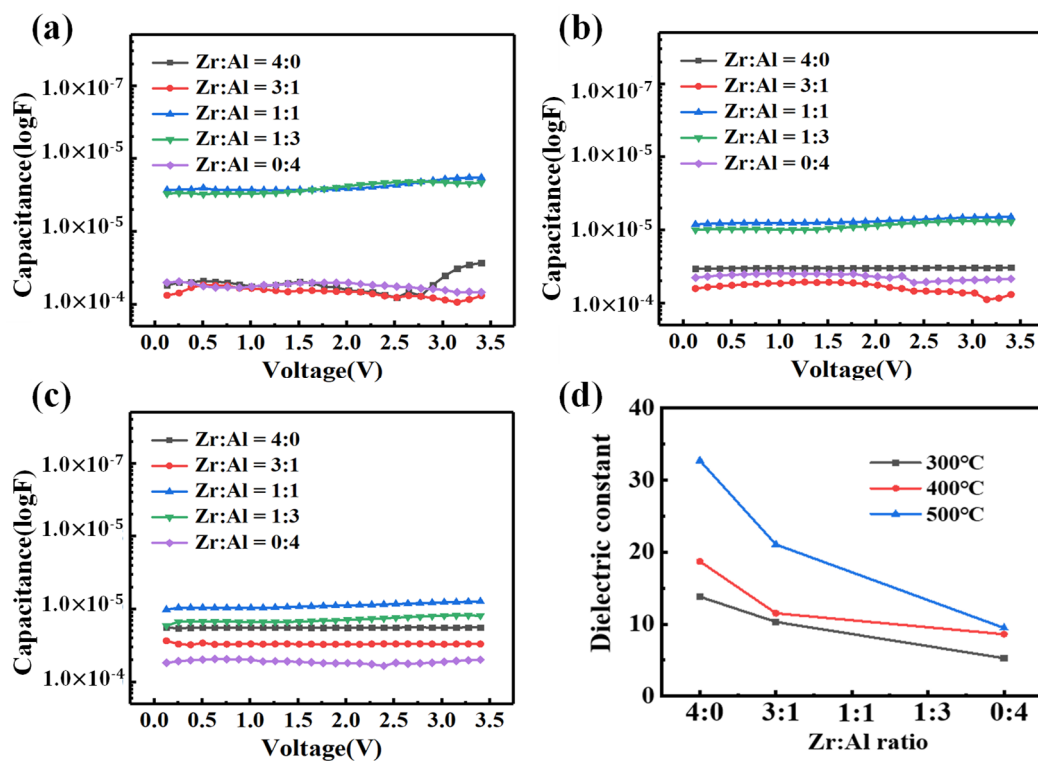


**Figure 8.** The capacitance of the ZAO films with altering ratios annealed at: (a) 300 °C; (b) 400 °C; and (c) 500 °C; as well as (d) the relative dielectric constants of the ZAO films changing with the mixing ratio of zirconia and alumina annealed at 400 and 500 °C.

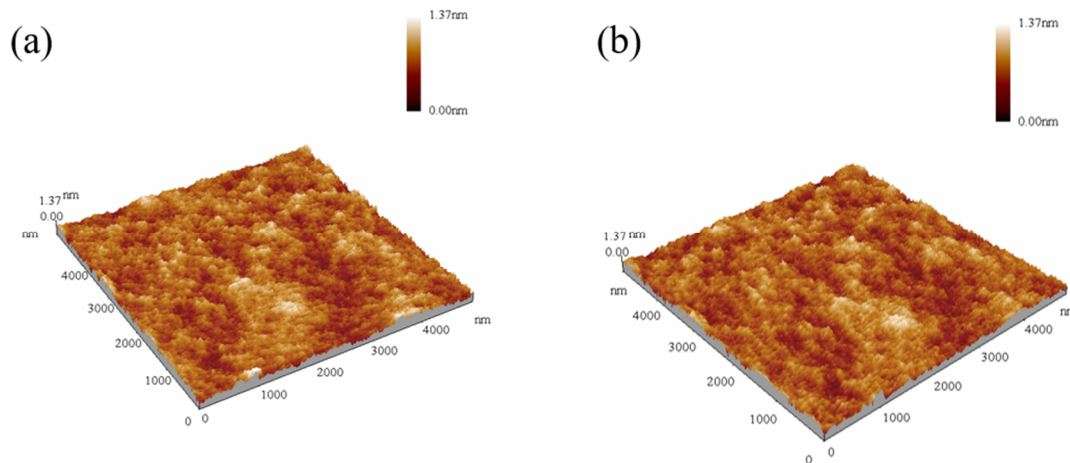
**Table 3.** The relationship among the thin film relative dielectric constants, mixing ratio and annealing temperature.

Molar Ratio Zr:Al	Relative Dielectric Constant at 300 °C	Relative Dielectric Constant at 400 °C	Relative Dielectric Constant at 500 °C
4:0	13.8	18.7	32.7
3:1	10.3	11.5	21.1
1:1	292	90.5	70.5
1:3	277	59.3	41.1
0:4	5.26	8.59	9.46

As a result, only with a molar ratio of Zr:Al = 3:1 can films obtain the high dielectric constants and the relatively low leakage current simultaneously. Moreover, we performed AFM measurements on the films and compared the roughness of the films under various preparation conditions, as shown in Table 4. It was shown that except for the high roughness of pure zirconium films due to crystallization at 400 and 500 °C, other films have a roughness of 0.1 to 0.3 nm, and the films annealed at 400 and 500 °C with a ratio of Zr:Al = 3:1 attained the smoothest surface ( $R_s = 0.14$  and  $0.15$  nm). The AFM images of the films are shown in Figure 9. With low roughness, the films are even and smooth, so the ZAO films can be well-combined with other parts of the TFT device. Thus, we prepared the dielectric layers with the ratio of Zr:Al = 3:1 at annealing temperatures of 400 and 500 °C, which were applied to the IGZO-TFT.

**Table 4.** The roughness of the films calculated from the AFM results.

Molar Ratio Zr:Al	Roughness at 300 °C/nm	Roughness at 400 °C/nm	Roughness at 500 °C/nm
4:0	0.19	0.48	0.60
3:1	0.30	0.14	0.15
1:1	0.26	0.22	0.22
1:3	0.33	0.31	0.43
0:4	0.31	0.37	0.30

**Figure 9.** The AFM images of the ZAO films with a ratio of Zr:Al = 3:1 annealed at (a) 400 °C and (b) 500 °C.

The prepared TFTs were tested at room temperature by a semiconductor parameter analyzer to obtain output curves and transfer characteristic curves. The saturation mobility and subthreshold swing of the thin-film transistor device were calculated from Equations (2) and (3) [46]:

$$I_{ds} = \frac{1}{2} \frac{W}{L} \mu C_i (V_{gs} - V_{th})^2 \quad (4)$$

$$SS = \frac{dV_{gs}}{d \log I_{ds}} \quad (5)$$

The result is shown in Figure 10. It can be calculated from Figure 10 that there is a mobility of 4.23 cm<sup>2</sup>/Vs under 400 °C annealing conditions, a subthreshold swing of 0.11 V/dec and an on/off ratio of 2.2 × 10<sup>6</sup>. Under 500 °C annealing conditions, there is a mobility of 14.89 cm<sup>2</sup>/Vs, a subthreshold swing of 0.11 V/dec and an on/off ratio of 6.1 × 10<sup>6</sup>. What's more, the TFT devices with pure zirconia or alumina films were fabricated, and the electric properties were summarized in Table 5 with a comparison between the pure films and the ZAO films. As a result, devices perform better with a higher annealing temperature. Therefore, the TFT with the ZAO films (ratio of Zr:Al = 3:1) annealed at 500 °C had the best electric properties. With ZAO-mixed film as dielectric layer, a device with good electrical properties can be obtained.

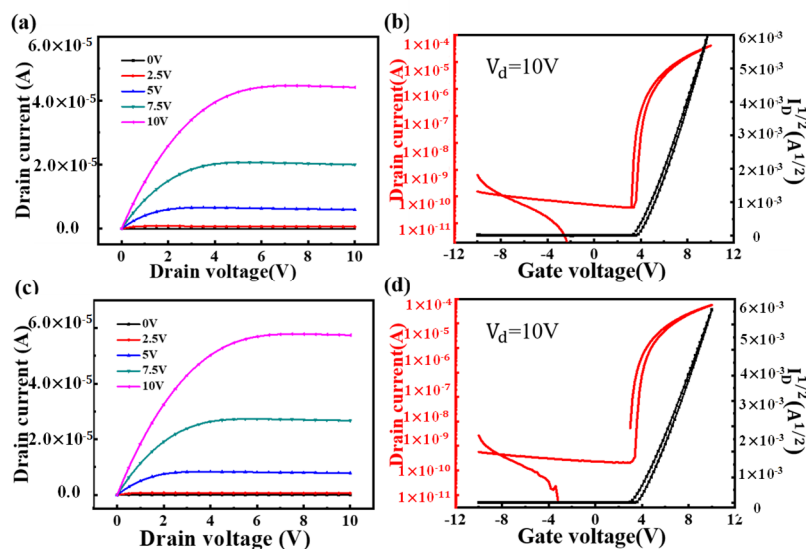


**Figure 10.** (a) Output curves of IGZO/ZAO (Zr:Al = 3:1) TFT at 400 °C; (b) transfer curves of IGZO/ZAO (Zr:Al = 3:1) TFT at 400 °C; (c) output curves of IGZO/ZAO (Zr:Al = 3:1) TFT at 500 °C; and (d) transfer curves of IGZO/ZAO (Zr:Al = 3:1) TFT at 500 °C.

**Table 5.** Electric characteristics of the devices.

Molar Ratio Zr:Al	Annealed at 400 °C			Annealed at 500 °C		
	$\mu_{sat}/cm^2/Vs$	$I_{on/off}$	SS(V/dec)	$\mu_{sat}/cm^2/Vs$	$I_{on/off}$	SS(V/dec)
4:0	1.21	$1.76 \times 10^7$	0.131	3.57	$3.5 \times 10^5$	0.22
3:1	4.23	$2.2 \times 10^6$	0.11	14.89	$6.1 \times 10^6$	0.11
1:1	13.04	$4.4 \times 10^3$	0.98	5.67	$2.73 \times 10^5$	0.27
1:3	10.18	$3.5 \times 10^4$	0.207	7.64	$6.4 \times 10^4$	0.42
0:4	6.58	$5.1 \times 10^6$	0.172	8.97	$1.61 \times 10^7$	0.35

### 4. Conclusions

In this study, we investigated the interaction between zirconia and alumina by conducting various tests on different mixing ratios of ZAO films and pure oxide films annealed at 300, 400 and 500 °C. It turns out that above the crystallization temperature of zirconia, mixing with the alumina can prevent the crystallization of the films and increase the optical bandgap, leading to a reduction in the leakage current density. Furthermore, as for pure alumina films, mixing with the zirconia inhibits the formation of oxygen defects, resulting in a higher dielectric constant. As a result, films with a ratio of Zr:Al = 3:1 maximally combine the advantages of the zirconia and alumina, achieving a high relative dielectric of 21.1 constant and a relatively low leakage current density of  $2.5 \times 10^{-6} A/cm^2@1MV/cm$ . Therefore, we fabricated the IGZO-TFT with optimal ZAO films annealed at 500 °C, which afforded a mobility of  $14.89 cm^2/Vs$ , a subthreshold swing of 0.11 V and an on/off ratio of  $6.1 \times 10^6$ .

**Author Contributions:** Conceptualization, Z.L. and S.Z.; Data curation and Formal analysis, W.Y.; Z.L., X.F. and J.C.; Project administration and Writing—original draft, Z.L.; Writing—review & editing, Z.L., W.C. and H.N.; Investigation Methodology, S.Z. and W.C.; Visualization, Z.Z.; Funding acquisition, X.F.; Resources, Software, Supervision, H.N., R.Y. and J.P. All authors have read and agreed to the published version of the manuscript.

**Funding:** This work was supported by Key-Area Research and Development Program of Guangdong Province (No. 2019B010934001), National Natural Science Foundation of China (Grant No. 51771074, 61804029 and 61574061), the Major Integrated Projects of National Natural Science Foundation of China (Grant No. U1601651), the Basic and Applied Basic Research Major Program of Guangdong Province (No. 2019B030302007), the Guangdong Natural Science Foundation (No. 2018A030310353), Science and Technology Project of Guangzhou (No. 201904010344), the Fundamental Research Funds for the Central Universities (No. 2019MS012), 2019 Guangdong University Student Science and Technology Innovation Special Fund (“Climbing Plan” Special Fund) (No. pdjh2019a0028 and pdjh2019b0041), National College Students’ Innovation and Entrepreneurship Training

Program (No. 201910561005 and 201910561007), South China University of Technology 100 Step Ladder Climbing Plan Research Project (No. j2tw201902475 and j2tw201902203) and the Open Project of Guangdong Province Key Lab of Display Material and Technology (No. 2017B030314031).

**Conflicts of Interest:** All authors have read and approve this version of the article, and due care has been taken to ensure the integrity of the work. No part of this paper has published or submitted elsewhere. No conflict of interest exists in the submission of this manuscript. The funders had no role in the design of the study; in the collection, analyses, or interpretation of data; in the writing of the manuscript, or in the decision to publish the results

## References

1. Yabuta, H.; Masafumi, S.; Katsumi, A.; Toshiaki, A.; Tohru, D.; Hideya, K. High-mobility thin-film transistor with amorphous InGaZnO<sub>4</sub> channel fabricated by room temperature rf-magnetron sputtering. *Appl. Phys. Lett.* **2006**, *89*, 112123. [[CrossRef](#)]
2. Powell, M.J. The physics of amorphous-silicon thin-film transistors. *IEEE Trans. Electron Devices* **1989**, *36*, 2753–2763. [[CrossRef](#)]
3. Park, J.S.; Maeng, W.-J.; Kim, H.-S.; Park, J.-S. Review of recent developments in amorphous oxide semiconductor thin-film transistor devices. *Thin Solid Films* **2012**, *520*, 1679–1693. [[CrossRef](#)]
4. Lin, C.-C. Effects of screen luminance combination and text color on visual performance with TFT-LCD. *Int. J. Ind. Ergon.* **2005**, *35*, 229–235. [[CrossRef](#)]
5. Katayama, M. Tft-lcd technology. *Thin Solid Films* **1999**, *341*, 140–147. [[CrossRef](#)]
6. Gao, Y.; Xu, Y.; Lu, J.; Zhang, J.; Li, X. Solution processable amorphous hafnium silicate dielectrics and their application in oxide thin film transistors. *J. Mater. Chem. C* **2015**, *3*, 11497–11504. [[CrossRef](#)]
7. Kwon, J.-Y.; Jung, J.S.; Son, K.S.; Lee, K.-H.; Park, J.S.; Kim, T.S.; Park, J.-S.; Choi, R.; Jeong, J.K.; Koo, B.; et al. The impact of gate dielectric materials on the light-induced bias instability in Hf-In-Zn-O thin film transistor. *Appl. Phys. Lett.* **2010**, *97*, 183503. [[CrossRef](#)]
8. Prins, M.; Grosse-Holz, K.-O.; Müller, G.; Cillessen, J.F.M.; Giesbers, J.B.; Weening, R.P.; Wolf, R.M. A ferroelectric transparent thin-film transistor. *Appl. Phys. Lett.* **1996**, *68*, 3650–3652. [[CrossRef](#)]
9. Yang, S.; Cho, D.-H.; Ryu, M.K.; Park, S.-H.K.; Hwang, C.-S.; Jang, J.; Jeong, J.K. Improvement in the photon-induced bias stability of Al-Sn-Zn-In-O thin film transistors by adopting AlO<sub>x</sub> passivation layer. *Appl. Phys. Lett.* **2010**, *96*, 213511. [[CrossRef](#)]
10. Byun, H.-R.; You, E.-A.; Ha, Y.-G. Room-temperature solution-processed, ZrO<sub>x</sub>-based hybrid gate dielectrics for low-voltage organic thin-film transistors on plastic substrates. *Appl. Phys. Lett.* **2019**, *114*, 013301. [[CrossRef](#)]
11. Fan, C.; Liu, A.; Meng, Y.; Guo, Z.; Liu, G.; Shan, F. Solution-processed SrO<sub>x</sub>-gated oxide thin-film transistors and inverters. *IEEE Trans. Electron Devices* **2017**, *64*, 4137–4143. [[CrossRef](#)]
12. Nayak, P.K.; Hedhili, M.N.; Cha, D.; Alshareef, H.N. High performance In<sub>2</sub>O<sub>3</sub> thin film transistors using chemically derived aluminum oxide dielectric. *Appl. Phys. Lett.* **2013**, *103*, 033518. [[CrossRef](#)]
13. Wei, C.-Y.; Adriyanto, F.; Lin, Y.-J.; Li, Y.-C.; Huang, T.-J.; Chou, D.-W.; Wang, Y.-H. Pentacene-based thin-film transistors with a solution-process hafnium oxide insulator. *IEEE Electron Device Lett.* **2009**, *30*, 1039–1041. [[CrossRef](#)]
14. Banger, K.; Yamashita, Y.; Mori, K.; Peterson, R.L.; Leedham, T.; Rickard, J.; Siringhaus, H. Low-temperature, high-performance solution-processed metal oxide thin-film transistors formed by a ‘sol-gel on chip’ process. *Nat. Mater.* **2011**, *10*, 45. [[CrossRef](#)] [[PubMed](#)]
15. Jeong, W.H.; Kim, G.H.; Shin, H.S.; Ahn, B.D.; Kim, H.J.; Ryu, M.-K.; Park, K.-B.; Seon, J.-B.; Lee, S.Y. Investigating addition effect of hafnium in InZnO thin film transistors using a solution process. *Appl. Phys. Lett.* **2010**, *96*, 093503. [[CrossRef](#)]
16. Rim, Y.S. Effect of Zr addition on ZnSnO thin-film transistors using a solution process. *Appl. Phys. Lett.* **2010**, *97*, 233502. [[CrossRef](#)]
17. Seo, S.-J.; Choi, C.G.; Hwang, Y.H.; Bae, B.-S. High performance solution-processed amorphous zinc tin oxide thin film transistor. *J. Phys. D Appl. Phys.* **2008**, *42*, 035106. [[CrossRef](#)]
18. Han, S.-Y.; Herman, G.S.; Chang, C.-H. Low-temperature, high-performance, solution-processed indium oxide thin-film transistors. *J. Am. Chem. Soc.* **2011**, *133*, 5166–5169. [[CrossRef](#)]

19. Hwang, S.; Lee, J.H.; Woo, C.H.; Lee, J.Y.; Cho, H.K. Effect of annealing temperature on the electrical performances of solution-processed InGaZnO thin film transistors. *Thin Solid Films* **2011**, *519*, 5146–5149. [[CrossRef](#)]
20. Shimoda, T.; Matsuki, Y.; Furusawa, M.; Aoki, T.; Yudasaka, I.; Tanaka, H.; Iwasawa, H.; Wang, D.; Miyasaka, M.; Takeuchi, Y. Solution-processed silicon films and transistors. *Nature* **2006**, *440*, 783. [[CrossRef](#)]
21. Young Choi, J.; Kim, S.S.; Lee, S.Y. Effect of hafnium addition on Zn-Sn-O thin film transistors fabricated by solution process. *Appl. Phys. Lett.* **2012**, *100*, 022109. [[CrossRef](#)]
22. Jeong, S.; Moon, J. Low-temperature, solution-processed metal oxide thin film transistors. *J. Mater. Chem.* **2012**, *22*, 1243–1250. [[CrossRef](#)]
23. Kim, H.; Kwack, Y.J.; Yun, E.J.; Choi, W.S. A mixed solution-processed gate dielectric for zinc-tin oxide thin-film transistor and its MIS capacitance. *Sci. Rep.* **2016**, *6*, 33576. [[CrossRef](#)] [[PubMed](#)]
24. Li, X.; Zhu, L.; Gao, Y.; Zhang, J. Solution-processed low-operating-voltage thin-film transistors with bottom-gate top-contact structure. *IEEE Trans. Electron Devices* **2015**, *62*, 875–881.
25. Jiang, S.; Yang, X.; Zhang, J.; Li, X. Solution-processed stacked TiO<sub>2</sub> and Al<sub>2</sub>O<sub>3</sub> dielectric layers for high mobility thin film transistor. *AIP Adv.* **2018**, *8*, 085109. [[CrossRef](#)]
26. Wu, W.; Javaid, K.; Liang, L.; Yu, J.; Liang, Y.; Song, A.; Yao, M.; Lan, L.; Cao, H. Aqueous Solution Induced High-Dielectric-Constant AlO<sub>x</sub>: Y Films for Thin-Film Transistor Applications. *J. Nanosci. Nanotechnol.* **2018**, *18*, 7566–7572. [[CrossRef](#)]
27. Avis, C.; Jang, J. High-performance solution processed oxide TFT with aluminum oxide gate dielectric fabricated by a sol-gel method. *J. Mater. Chem.* **2011**, *21*, 10649–10652. [[CrossRef](#)]
28. Xu, W.; Wang, H.; Xie, F.; Chen, J.; Cao, H.; Xu, J.B. Facile and environmentally friendly solution-processed aluminum oxide dielectric for low-temperature, high-performance oxide thin-film transistors. *ACS Appl. Mater. Interfaces* **2015**, *7*, 5803–5810. [[CrossRef](#)]
29. Sang, Y.L.; Chang, S.; Lee, J.-S. Role of high-k gate insulators for oxide thin film transistors. *Thin Solid Films* **2010**, *518*, 3030–3032.
30. Lee, C.-G.; Dodabalapur, A. Solution-processed high-k dielectric, ZrO<sub>2</sub>, and integration in thin-film transistors. *J. Electron. Mater.* **2012**, *41*, 895–898. [[CrossRef](#)]
31. Zhang, J.; Fu, X.; Zhou, S.; Ning, H.; Wang, Y.; Guo, D.; Cai, W.; Liang, Z.; Yao, R.; Peng, J. The Effect of Zirconium Doping on Solution-Processed Indium Oxide Thin Films Measured by a Novel Nondestructive Testing Method (Microwave Photoconductivity Decay). *Coatings* **2019**, *9*, 426. [[CrossRef](#)]
32. Scriven, L. Physics and applications of dip coating and spin coating. *MRS Online Proc. Libr. Arch.* **1988**, *121*. [[CrossRef](#)]
33. Stillwagon, L.; Larson, R. Leveling of thin films over uneven substrates during spin coating. *Phys. Fluids A Fluid Dyn.* **1990**, *2*, 1937–1944. [[CrossRef](#)]
34. Kato, K.; Saito, T.; Shibayama, S.; Sakashita, M.; Takeuchi, W.; Taoka, N.; Nakatsuka, O.; Zaima, S. Stabilized formation of tetragonal ZrO<sub>2</sub> thin film with high permittivity. *Thin Solid Films* **2014**, *557*, 192–196. [[CrossRef](#)]
35. Joy, K.; Berlin, I.J.; Nair, P.B.; Lakshmi, J.S.; Daniel, G.P.; Thomas, P.V. Effects of annealing temperature on the structural and photoluminescence properties of nanocrystalline ZrO<sub>2</sub> thin films prepared by sol-gel route. *J. Phys. Chem. Solids* **2011**, *72*, 673–677. [[CrossRef](#)]
36. Brenier, R.; Gagnaire, A. Densification and aging of ZrO<sub>2</sub> films prepared by sol-gel. *Thin Solid Films* **2001**, *392*, 142–148. [[CrossRef](#)]
37. Gao, Y.; Li, X.; Chen, L.; Shi, J.; Sun, X.; Zhang, J. High Mobility Solution-Processed Hafnium Indium Zinc Oxide TFT With an Al-Doped ZrO<sub>2</sub> Gate Dielectric. *IEEE Electron Device Lett.* **2014**, *35*, 554–556.
38. Yoo, Y.B.; Park, J.; Lee, K.H.; Lee, H.W.; Song, K.M.; Lee, S.J.; Baik, H.K. Solution-processed high-k HfO<sub>2</sub> gate dielectric processed under softening temperature of polymer substrates. *J. Mater. Chem. C* **2013**, *1*, 1651–1658. [[CrossRef](#)]
39. Jayaraj, M.K.; Kachirayil, J.; Saji, K.; Toshio, K.; Hideo, H. Optical and electrical properties of amorphous zinc tin oxide thin films examined for thin film transistor application. *J. Vac. Sci. Technol. B Microelectron. Nanometer Struct. Process. Meas. Phenom.* **2008**, *26*, 495–501. [[CrossRef](#)]
40. Shan, F.; Yu, Y. Band gap energy of pure and Al-doped ZnO thin films. *J. Eur. Ceram. Soc.* **2004**, *24*, 1869–1872. [[CrossRef](#)]
41. Umebayashi, T.; Yamaki, T.; Itoh, H.; Asai, K. Band gap narrowing of titanium dioxide by sulfur doping. *Appl. Phys. Lett.* **2002**, *81*, 454–456. [[CrossRef](#)]

42. Jung, Y.; Yang, W.; Koo, C.Y.; Songab, K.; Moon, J. High performance and high stability low temperature aqueous solution-derived Li–Zr co-doped ZnO thin film transistors. *J. Mater. Chem.* **2012**, *22*, 5390–5397. [[CrossRef](#)]
43. Yang, W.; Song, K.; Jung, Y.; Jeong, S.; Moon, J. Solution-deposited Zr-doped AlO<sub>x</sub> gate dielectrics enabling high-performance flexible transparent thin film transistors. *J. Mater. Chem. C* **2013**, *1*, 4275–4282. [[CrossRef](#)]
44. Park, J.H.; Kim, K.; Yoo, Y.B.; Park, S.Y.; Lim, K.-H.; Lee, K.H.; Baik, H.K.; Kim, Y.S. Water adsorption effects of nitrate ion coordinated Al<sub>2</sub>O<sub>3</sub> dielectric for high performance metal-oxide thin-film transistor. *J. Mater. Chem. C* **2013**, *1*, 7166–7174. [[CrossRef](#)]
45. Wu, J.; Nan, C.W.; Lin, Y.; Deng, Y. Giant dielectric permittivity observed in Li and Ti doped NiO. *Phys. Rev. Lett.* **2002**, *89*, 217601. [[CrossRef](#)]
46. Naik, B.R.; Avis, C.; Kim, T.; Jang, J. Improvement in performance of solution-processed indium–zinc–tin oxide thin-film transistors by UV/O<sub>3</sub> treatment on zirconium oxide gate insulator. In Proceedings of the International Workshop on Active-matrix Flatpanel Displays & Devices, Kyoto, Japan, 23–26 June 2016.



© 2020 by the authors. Licensee MDPI, Basel, Switzerland. This article is an open access article distributed under the terms and conditions of the Creative Commons Attribution (CC BY) license (<http://creativecommons.org/licenses/by/4.0/>).